# Measurements and correlations of turbulent burning velocities over wide ranges of fuels and elevated pressures

D. Bradley [a],[*], M. Lawes [a], Kexin Liu [b], M.S. Mansour [c]

[a] *School of Mechanical Engineering, University of Leeds, Leeds LS2 9JT, UK*
[b] *Siemens Industrial Turbomachinery (SIT) Ltd., Lincoln, UK*
[c] *Clean Combustion Research Center, King Abdullah University of Science and Technology, Thuwal, Saudi Arabia*

Available online 29 June 2012

**Abstract**

The implosion technique has been used to extend measurements of turbulent burning velocities over greater ranges of fuels and pressures. Measurements have been made up to 3.5 MPa and at strain rate Markstein numbers as low as −23. The implosion technique, with spark ignition at two opposite wall positions within a fan-stirred spherical bomb is capable of measuring turbulent burning velocities, at higher pressures than is possible with central ignition. Pressure records and schlieren high speed photography define the rate of burning and the smoothed area of the flame front. The first aim of the study was to extend the previous measurements with ethanol and propane–air, with further measurements over wider ranges of fuels and equivalence ratios with mixtures of hydrogen, methane, 10% hydrogen–90% methane, toluene, and *i*-octane, with air. The second aim was to study further the low turbulence regime in which turbulent burning co-exists with laminar flame instabilities.

Correlations are presented of turbulent burning velocity normalised by the effective rms turbulent velocity acting on the flame front, $u_t/u'_k$, with the Karlovitz stretch factor, $K$, for different strain rate Markstein numbers, a decrease in which increases $u_t/u'_k$. Experimental correlations are presented for the present measurements, combined with previous ones. Different burning regimes are also identified, extending from that of mixed turbulence/laminar instability at low values of $K$ to that at high values of $K$, in which $u_t/u'_k$ is gradually reduced due to increasing localised flame extinctions.
© 2012 The Combustion Institute. Published by Elsevier Inc. All rights reserved.

*Keywords:* Premixed turbulent flames; Turbulent burning velocity; High pressure; Turbulent/laminar flame instabilities; Explosion measurements

## 1. Introduction

Measurements of inwardly propagating explosion flame kernels enable burning velocities to be measured close to the safe working pressure of the explosion bomb. This implosion technique, with ignition at diametrically opposite spark electrodes has been employed to measure both laminar [1] and, in a fan-stirred bomb, turbulent [2] burning velocities. In the latter, pressure measurements and schlieren high speed flame photography define the smoothed area of the turbulent

* Corresponding author. Fax: +44 113 343 2150.
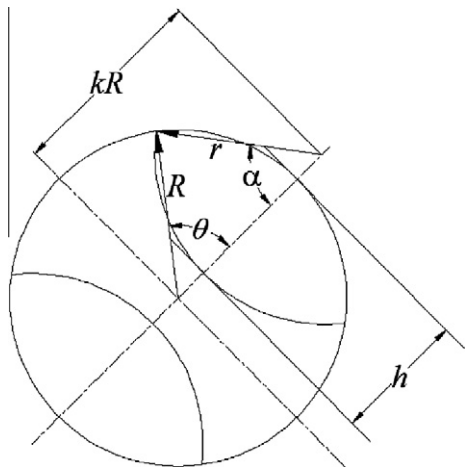  *E-mail address:* d.bradley@leeds.ac.uk (D. Bradley).

Fig. 1. Configuration of twin kernels with key dimensions.



Fig. 2. Variations of $u_t$ with $p$ (lower scale) and $T$ (upper scale) for stoichiometric mixtures of three fuels at $p_o = 1.0$ MPa, with $u' = 1$ and 2 m/s.

flame front and the mass rate of burning during the implosions, to yield associated values of turbulent burning velocity, $u_t$.

Over a wide range of conditions the ratio of $u_t$, to the effective rms turbulent velocity, $u_t/u'_k$, that allows for the development of the flame kernel, can be expressed in terms of the Karlovitz stretch factor, $K$, by [2,3]:

$$u_t/u'_k = U = \alpha K^\beta \quad \text{for } K > 0.05. \tag{1}$$

$\alpha$ and $\beta$ are constants expressed by first order expressions in terms of the strain rate Markstein number, $Ma_{sr}$. $K$ is given by [3]:

$$K = 0.25(u'/u_\ell)^2 R_l^{-0.5}, \tag{2}$$

where $u'$ is the measured rms turbulent velocity and $R_l$ the turbulent Reynolds number, $u'l/v$, with $l$ the integral turbulence length scale and $v$ the kinematic viscosity.

The study has two principal aims. The first is to measure $u_t$ with five additional and contrasting fuels at different pressures and equivalence ratios, $\phi$, to ascertain whether Eq. (1) is generally applicable. The range of $Ma_{sr}$ values is extended from $-11$ to 3 in [2] to $-23$ to 5. This parameter is important, in that it expresses fuel effects arising from flame stretch sensitivities. The maximum laminar flame speed has been similarly used as a correlating parameter in [4]. The second aim is
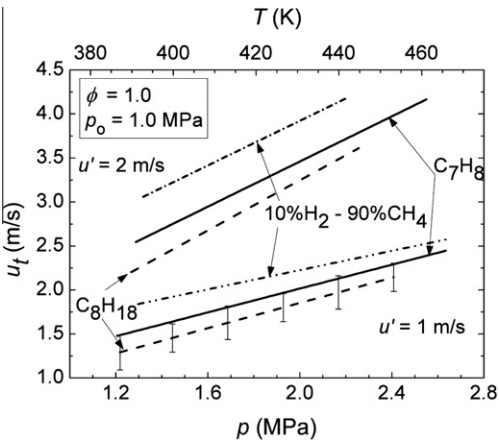
to study the regime of $K < 0.1$, in which there is strong evidence of coupling between turbulence and laminar flame instabilities, giving increased values of $U$ [5,6]. The fuels in [2,3] were ethanol and propane and in the present study, hydrogen, methane, toluene and *i*-octane, up to a maximum pressure of 3.5 MPa and 480 K.

## 2. Experimental method

Key dimensions are represented for the propagating flame kernels on Fig. 1. Turbulent flame surfaces are represented by smoothed spherical surfaces, with the mass of unburned gas within the surface equal to the mass of burned gas outside it. The surface is defined in relation to the schlieren front. The centre of the curvature of the smoothed flame front, of flame radius $r$, is usually outside the inner wall of the spherical bomb. The complete analysis leading to the derivation of $u_t$, assumed to be the same for both kernels, is given in [2]. The mass burned, $m_u$, is deduced from the flame front geometry. This must be compatible with that deduced from the measured pressure, $p$. Values of $k$, which controls the position of the centre of the flame cusp radius, see Fig. 1, for each kernel were fine-tuned to achieve this. The area of each single flame surface was found and this together with $dm_u/dt$, yielded [2]:

Table 1
Ranges of experimental parameters in present study, pressure in MPa and $u'$ in m/s.

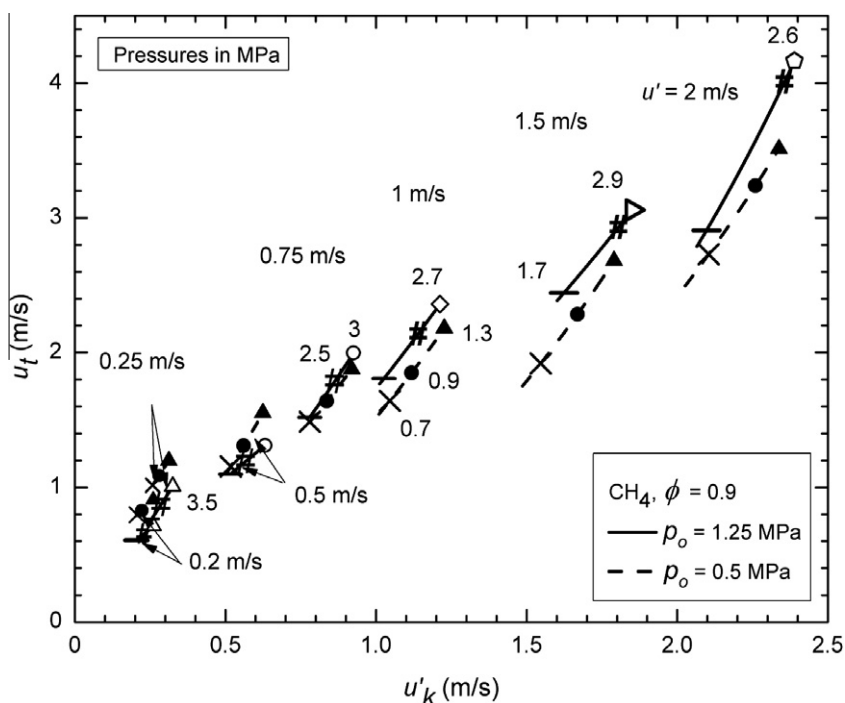|         | H$_2$              | CH$_4$                     | C$_7$H$_8$  | C$_8$H$_{18}$ | 10% H$_2$–90% CH$_4$ |
|---------|--------------------|----------------------------|-------------|---------------|----------------------|
| $\phi$  | 0.3,0.4,0.5,0.6,0.8 | 0.9                        | 1.0,1.2     | 1.0,1.4       | 0.8, 1.0,1.2         |
| $p_o$   | 0.5,0.7,1.0        | 0.1,0.5,0.75,1.0,1.25      | 0.5,0.75,1.0 | 0.5,1.0       | 0.5,0.75,1.0         |
| $u'$    | 1,2,3,4            | 0.2,0.25,0.5,0.75,1,1.5,2  | 1,2,3,4     | 1,2,3         | 1,2                  |

Fig. 3. Variations of $u_t$ with $u'_k$ for CH$_4$–air, $\phi = 0.9$, $p_o = 0.5$ and 1.25 MPa, for different $u'$. Solid and broken lines are best fit curves. Values of velocity are for $u'$. Each large symbol represents a particular pressure in MPa, indicated by an adjacent number.



Fig. 4. Variations of $u_t$ with $u'_k$ for different lean H$_2$–air mixtures, $\phi = 0.4$, 0.6 and 0.8, $p_o = 1.0$ MPa and different $u'$. Solid and broken lines are best fit curves. Values of velocity are for $u'$. Each large symbol represents a particular pressure in MPa, indicated by an adjacent number.
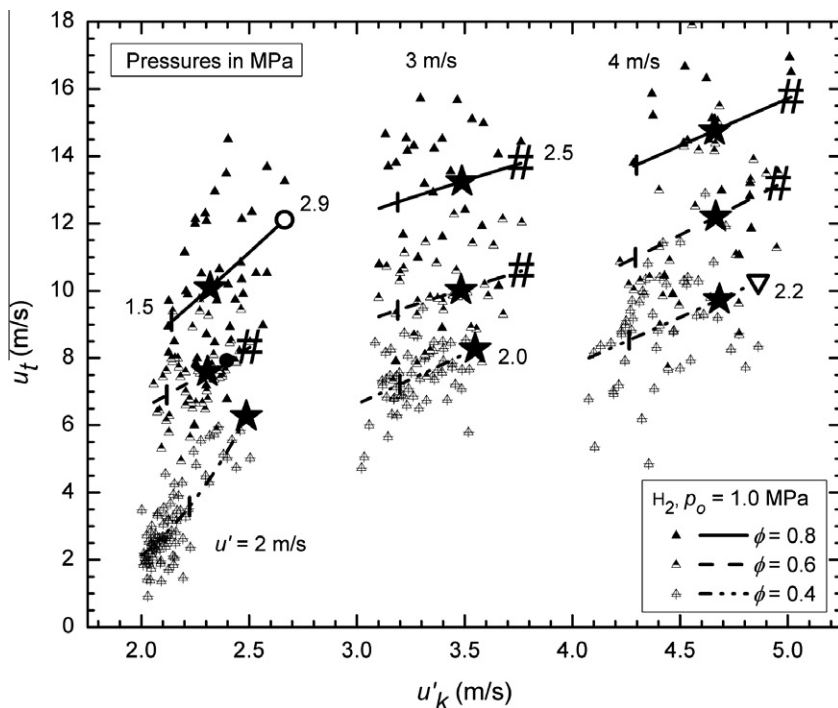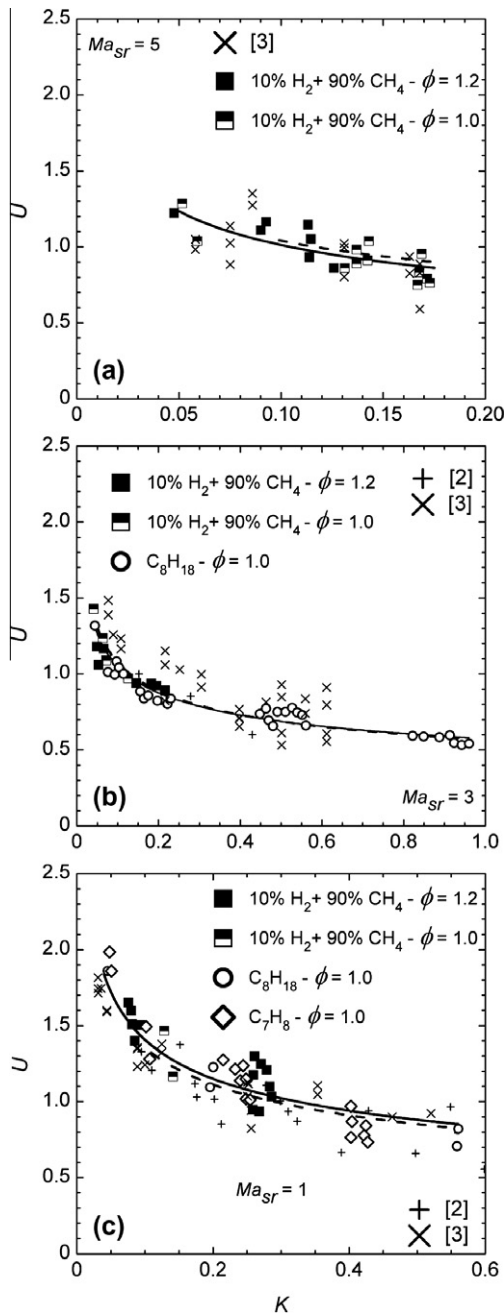
Fig. 5. Correlations of present measurements for positive $Ma_{sr}$, $K > 0.05$. Full line curves are best fit curves. Broken curves express Eqs. (1), (4), and (5), for $K \geqslant 0.1$. Cross and multiplication symbols are from data in [2] and [3].

$$u_t = \frac{(4/3)\pi R_o^3}{(p_e - p_o)} \frac{(\rho_o/\rho_u)dp/dt}{\sum 2\pi r^2 (1 - \cos \alpha)}. \qquad (3)$$

$\sum$ indicates the summation of both flame areas, $p_o$ original pressure, $p_e$ at the end of the explosion, $\rho_o$

original density, and $\rho_u$ unburned gas density at pressure, $p$. In [2] it is shown that $\cos \alpha = ((k^2 - 1 + (r/R)^2)/2k(r/R))$.

The spherical stainless steel bomb has an internal radius, $R$, of 190 mm. That of a sphere with the same internal volume as the bomb, $R_0$, is 192.78 mm. It has three pairs of orthogonal windows of 150 mm diameter. Turbulence was generated by four identical, fans, located close to the wall, each driven by a directly coupled electric motor with independent speed control. The fans were in a regular tetrahedron configuration, to create a central region of uniform, isotropic turbulence, with $u'$ measured by laser doppler velocimetry and the integral length scale, $l = 20$ mm, by two point correlation.

In its early stages the flame is only wrinkled by the smaller wavelengths of the turbulent spectrum, with an effective rms at the flame front of $u'_k$ [3], with $u'_k/u'$ found from integration of the turbulent power spectral density function between the limiting wave numbers [7]. Rapid compression of unburned gas decreases the length scale below the initial value and conservation of angular momentum increases $u'_k$ [8]. Allowances were made for these, as well as the small effect of the changes in $l$ and $u'$, on values of $K$ [3].

Electric heaters at the wall provided up to 6 kW for preheating the vessel and mixture up to 358 K, measured by a thermocouple. Gaseous mixtures were made directly in the bomb using partial pressures, whilst liquid fuels were metered and introduced using a syringe. Complete evaporation was checked from partial pressures. Pressures were measured with a Kistler pressure transducer. Ignitions occurred simultaneously at two diametrically opposite spark plugs, with spark gaps 11 mm from the inside wall, with energies of about 23 mJ. Flame front propagations were observed by schlieren photography, using a high speed, Phantom digital camera, synchronised with the pressure measurements.

The camera had 256 Megabytes integral image memory and framing rates of 6300 and 9000 frames/s with pixels of 480 × 480 and 384 × 384 and respective resolutions of 0.3986 and 0.4065 mm/pixel. Further details are in [2,9].

## 3. Experimental results

Experimental conditions are summarised in Table 1. Figure 2 shows variations of $u_t$ with $p$ for stoichiometric mixtures of three fuels, for $p_o = 1.0$ MPa, with $u' = 1$ and 2 m/s. The top scale gives the unburned gas temperature for isentropic compression from the GasEq Code [10]. These compressions result in linear increases in $u_t$ with pressure, with the highest values for the hydrogen/methane mixture. Values of $u_t$ are means derived from five explosions, with one typical spread of values indicated by vertical lines.
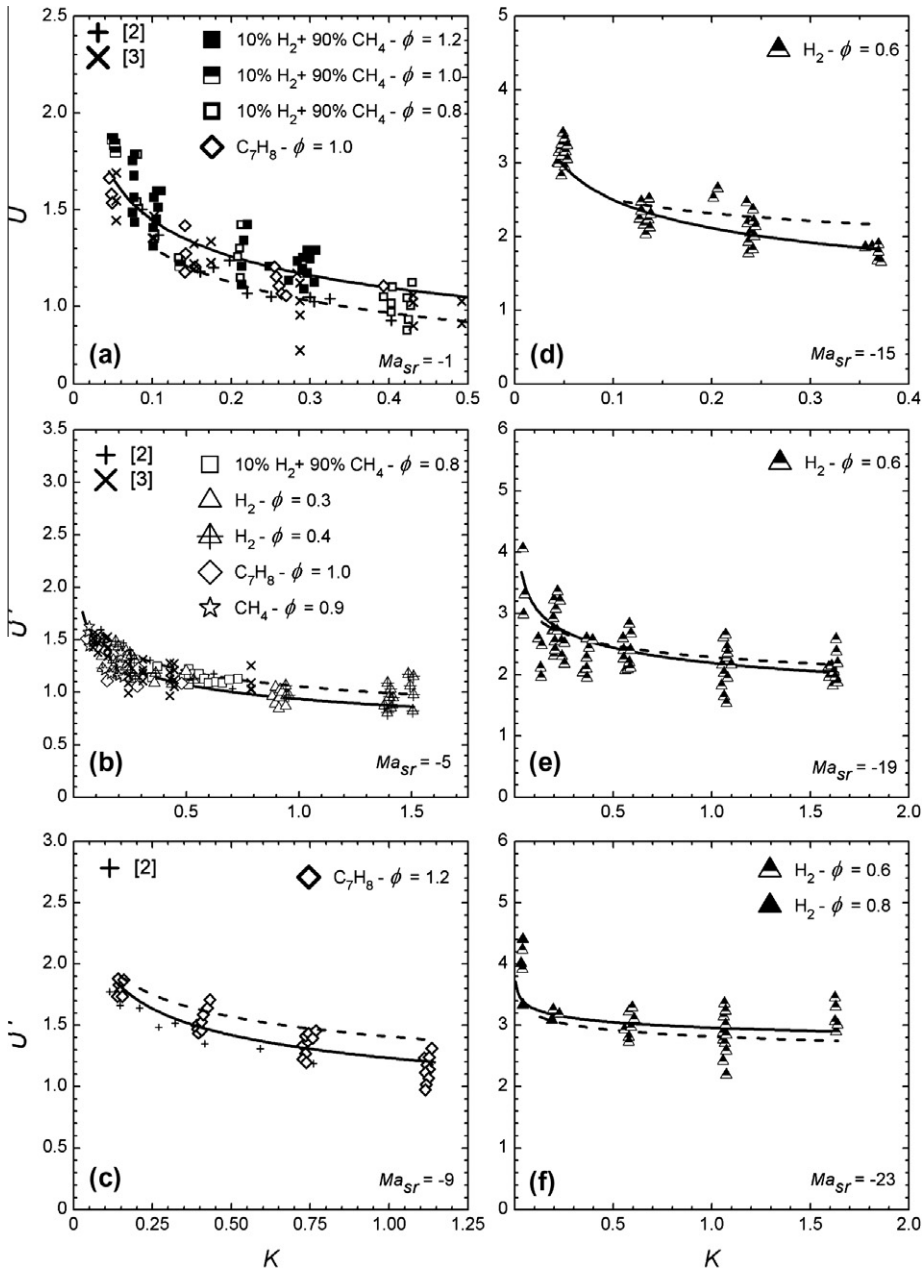
Fig. 6. Correlations of present measurements for negative $Ma_{sr}$, $K > 0.05$. Full line curves are best fit curves. Broken curves express Eqs. (1), (4), and (5), for $K \geqslant 0.1$. Cross and multiplication symbols are from data in [2] and [3].

Variations of $u_t$ with $u'_k$ during implosions are given in Figs. 3 and 4. Figure 3 is for CH₄–air, with initial pressures of $p_o = 0.5$ and 1.25 MPa for $\phi = 0.9$, and at different $u'$. Figure 4 is for hydrogen–air mixtures, $p_o = 1.0$ MPa, with $\phi = 0.4$, 0.6 and 0.8, also at different $u'$. Different symbols show the scatter in $u_t$, while the lines represent the best fit.

Values of $u_t$ increase linearly with $u'_k$ in Figs. 3 and 4, up to 3.5 MPa. For the lean H₂ mixtures in Fig. 4, values of $u_t$ at a given $u'_k$ tend to increase with $\phi$, as $Ma_{sr}$ decreases. Space limitations preclude the presentation of all the experimental data, but these are available from the corresponding author.

## 4. Discussion of results

### 4.1. Fully turbulent regime, K > 0.1

Experimental points, from the data in Figs. 2–4 and additional data, are plotted on Fig. 5a–c for positive values of $Ma_{sr}$. Plots for negative $Ma_{sr}$ are given in Fig. 6a–f. Sources for $u_\ell$ and $Ma_{sr}$ are referenced in Table 2. For toluene and the hydrogen–methane mixtures these were obtained directly from centrally ignited laminar flame measurements up to 1.0 MPa and 358 K. Error bands on values of $Ma_{sr}$ are usually about ±1. Extrapolations were necessary to obtain values at the higher temperatures and pressures of the implosions. As in previous studies, mass burning velocities, $u_t$, are those associated with the smoothed flame surface, where the mean reaction progress variable is close to 0.59.

Full line curves in Figs. 5 and 6 are best fits to the data points, in terms of "$R^2$" values. From these, expressions were derived for each value of $Ma_{sr}$, for the optimal correlation of all the experimental points. Based on all the present measurements and those in [2,3], these expressions are:

For positive values of $Ma_{sr}$, $\alpha$

$$= 0.023(30 - Ma_{sr}) \quad \text{and} \quad \beta$$
$$= 0.0103(Ma_{sr} - 30), \tag{4}$$

and

#### Table 2
Values of $u_\ell$ (m/s) and $Ma_{sr}$ for mixtures in present study.

| $p$ | H$_2$ [11] | | | | | |
|---|---|---|---|---|---|---|
| | 1.0 | | 2.0 | | 3.0 | |
| $\phi$ | $u_\ell$ | $Ma_{sr}$ | $u_\ell$ | $Ma_{sr}$ | $u_\ell$ | $Ma_{sr}$ |
| 0.3 | 0.08 | −5.59 | 0.06 | −5.77 | 0.05 | −5.87 |
| 0.4 | 0.21 | −5.94 | 0.15 | −6.12 | 0.13 | −6.22 |
| 0.5 | 0.39 | −7.19 | 0.29 | −7.37 | 0.24 | −7.47 |
| 0.6 | 0.80 | −13.4 | 0.64 | −18.9 | 0.56 | −22.2 |
| 0.8 | 1.42 | −13.8 | 1.23 | −20.0 | 1.13 | −23.6 |
| | CH$_4$ [12] | | | | | |
| 0.9 | 0.17 | −3.57 | 0.14 | −5.69 | 0.13 | −6.93 |
| | C$_7$H$_8$ [present work] | | | | | |
| 1.0 | 0.19 | 0.47 | 0.19 | −4.32 | 0.19 | −7.13 |
| 1.2 | 0.13 | −5.51 | 0.12 | −10.5 | 0.11 | −13.4 |
| | i-C$_8$H$_{18}$ [13,14] | | | | | |
| 1.0 | 0.25 | 3.13 | 0.23 | 2.22 | 0.22 | 1.68 |
| 1.4 | 0.11 | 2.35 | 0.1 | 2.04 | 0.1 | 2.06 |
| | 10% H$_2$–90% CH$_4$ [present work] | | | | | |
| 0.8 | 0.23 | 4.06 | 0.17 | −0.71 | 0.14 | −5.48 |
| 1.0 | 0.23 | 4.61 | 0.18 | 0.75 | 0.16 | −3.12 |
| 1.2 | 0.13 | 1.32 | 0.1 | 1.07 | 0.08 | 0.92 |

for negative values of $Ma_{sr}$, $\alpha$

$$= 0.085(7 - Ma_{sr}) \quad \text{and} \quad \beta$$
$$= -0.0075(Ma_{sr} + 30). \tag{5}$$

The broken curves on Figs. 5 and 6 express Eqs. (1), (4), and (5). Despite some scatter, bearing in mind the uncertainty in values of $Ma_{sr}$, the data are represented satisfactorily by these three expressions.

### 4.2. Regime of mild turbulence and laminar instabilities, K < 0.1

At low values of $u'$ the flame remains laminar-like and susceptible to laminar flame instabilities [5,6,15]. For $K < 1$ values of $U$ are plotted against $K$ logarithmically for three values of $Ma_{sr}$ in Fig. 7. Values of $U$ peak, over quite narrow ranges of $K$. At very low values of $K$ the parameter, $U$, becomes less informative, as $u' \to 0$, $U \to \infty$ and $U$ might better be replaced by the unstable laminar burning velocity normalised by $u_\ell$ [1]. Peak values of $U$ are analysed in terms of the interplay of the smallest wavelengths of a reacting turbulent eddy on the Gibson length scale, $l_G$, and that of the Darrieus–Landau, thermo-diffusive laminar instability, $l_s$, at the inner cut-off [1].

Let $l_s$ be normalised by the flame thickness, $\delta_\ell = v/u_\ell$, to give $\Lambda_s$, which depends upon $Ma_{sr}$. For the three mixtures in Fig. 7 values from planar fluorescence measurements in [16], are listed in Table 3. It is readily shown that:

$$l_s/l = \Lambda_s(u'/u_\ell)R_l^{-1}. \tag{6}$$

In [17,18] $l_G$ is given by:

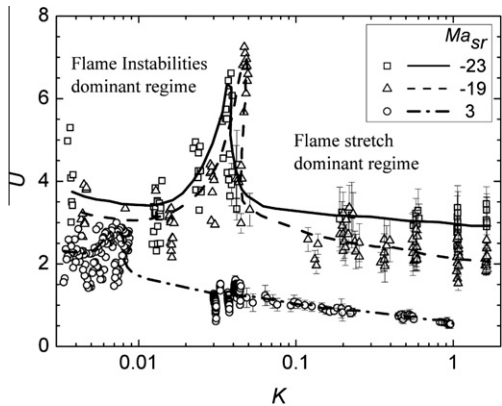$$l/l_G = (2u'/u_\ell)^3. \tag{7}$$

From Eqs. (6) and (7)



Fig. 7. Correlation for $K < 0.1$, showing increased $U$ due to turbulent/unstable laminar flame interactions.

Table 3
Initiation and termination of instability.

| $Ma_{sr}$ | $\Lambda_s$ [16] | Initiation | | Maximum value | | Termination | |
|---|---|---|---|---|---|---|---|
| | | $K_i$ | $l_s/l_G$ | $K_m$ | $l_s/l_G$ | $K_t$ | $l_s/l_G$ |
| 3 | 2270 | 0.004 | 4.6 | 0.0073 | 15.5 | 0.009 | 23.5 |
| −19 | 50 | 0.011 | 0.77 | 0.048 | 14.7 | 0.07 | 31.4 |
| −23 | 50 | 0.012 | 0.64 | 0.045 | 13.0 | 0.064 | 26.2 |

$$l_s/l_G = 8\Lambda_s(u'/u_\ell)^4 R_l^{-1}, \tag{8}$$

and from Eq. (2)

$$l_s/l_G = 128\Lambda_s K^2. \tag{9}$$

The wavelength ratio $l_s/l_G$ indicates the relative contributions of laminar flame instabilities and hydrodynamic turbulence to flame wrinkling. A small ratio indicates little wrinkling within the smallest unstable wavelength by the reacting turbulent eddies. A large ratio indicates extensive wrinkling, to the extent that turbulence finally dominates. The maximum value of $U$ of about 7 occurs when the combined wrinkling is greatest for the very negative values of $Ma_{sr}$. Values of $K$ at which increased flame wrinkling is initiated are indicated by $K_i$ in Table 3. Corresponding values of $l_s/l_G$ from Eq. (9), of approximate order unity, are shown in the next column. The following column shows values of $K$, namely $K_m$, at which $U$ is a maximum, with corresponding values of $l_s/l_G$, of about 15.

As $K$ increases further, $U$ declines, as the wrinkling from the growing turbulence wavelengths associated with increase in $u'$, dominates the flame wrinkling, with eradication of the influence of the original instability wavelength. Table 3 shows values of $K$, namely $K_t$, from Fig. 7, at which the enhancement of $U$ terminates. The associated values of $l_s/l_G$ range from about 23 to 31, with $K_t$ close to 0.1, for the two highly unstable mix-



Fig. 8. Regimes of turbulent combustion, showing extension of zone of unstable flamelets at increasing $K$ as $Ma_{sr}$ is reduced.

tures. This value is close to the limits for the termination of instability effects observed in [19,20] and plotted in [21]. Similarly, in the present work these effects terminated at $u_t/u_l > 3$, as previously observed experimentally in [22].

## 5. Conclusions

The correlation of turbulent burning velocities has been extended to cover 7 fuels at different equivalence ratios, $Ma_{sr}$ down to −23, and pressures up to 3.5 MPa. In Fig. 8 the full line curves represent the general correlations, Eqs. (1), (4), and (5), within their bounds of experimental validity. The broken curves are extensions beyond those bounds, up to the dotted curve. This curve identifies approximate points at which there is a probability of 0.8 of an initial flame kernel continuing to propagate, which is indicative of the onset of flame quenching at a value of $K$ identified by $K_{0.8}$. This limit curve is obtained from the correlation for $K_{0.8}$ in [23], but extends no lower than $Ma_{sr} = −3.0$. The upper dotted curve, at lower values of $K$, shows the inner limit for Eqs. (1), (4), and (5), created by $K_t$ when the coupling between turbulence and laminar instability appears to have ceased at the different values of $Ma_{sr}$. In zone A, at values of $K$ lower than these, the flames are subject to this coupling and $U$ reaches values as high as 7, when flame wrinkling due to both flame instabilities and turbulence is a maximum.

Zone B extends between $K$ values of $K_t$ and $K_{0.8}$. In the range $0.4 < K < 2$, at a given $Ma_{sr}$, very approximately $u_t$ is proportional to $u'_k$. The value of $u_t$ is primarily dependent on the amplitude of the flame wrinkling. The arrowed vertical line at constant $K$ indicates an increased rate of burning in laminar flamelets, independent of that due to flame wrinkling, as $Ma_{sr}$ is decreased in the predominantly positively stretched flames. This results in an increase in the localised laminar burning velocity in the flamelets. An additional factor is that a decrease in $Ma_{sr}$ appears to be associated with an increase in the extinction stretch rate [21].

Zone C is that in which $K > K_{0.8}$. Here, as flame quenching develops, flame fronts begin to lose their coherence and measurements of $u_t$ become progressively more difficult.
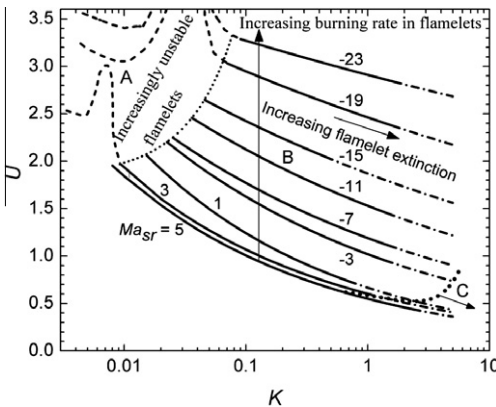
## Acknowledgement

## References

[1] A.S. Al-Shahrany, D. Bradley, M. Lawes, R. Woolley, *Proc. Combust. Inst.* 30 (2005) 225–232.

[2] D. Bradley, M. Lawes, M.S. Mansour, *Proc. Combust. Inst.* 33 (2011) 1269–1275.

[3] D. Bradley, M. Lawes, M.S. Mansour, *Combust. Flame* 158 (2011) 123–138.

[4] P.P. Venkateswaran, A. Marshall, Dong HyukShin, D. Noble, J. Seitzman, T. Lieuwen, *Combust. Flame* 158 (2011) 1602–1614.

[5] H. Kobayashi, T. Tamura, K. Maruta, T. Niioka, F.A. Williams, *Proc. Combust. Inst.* 26 (1996) 389–396.

[6] Derek Bradley, Malcolm Lawes, Morkous S. Mansour, *Flow Turbul. Combust.* 87 (2011) 191–204.

[7] D. Bradley, M. Lawes, M.S. Mansour, *Proc. Combust. Inst.* 32 (2009) 1587–1593.

[8] R.J. Tabaczynski, F.H. Trinker, B.A.S. Shannon, *Combust. Flame* 39 (1980) 111–121.

[9] D. Bradley, M.Z. Haq, R.A. Hicks, et al., *Combust. Flame* 133 (2003) 415–430.

[10] C. Morley, Gaseq Chemical Equilibrium Program, available at c.morley@ukgateway.net.

[11] D. Bradley, M. Lawes, Kexin Liu, S. Verhelst, R. Woolley, *Combust. Flame* 149 (2007) 162–172.

[12] X.J. Gu, M.Z. Haq, M. Lawes, R. Woolley, *Combust. Flame* 121 (2000) 41–58.

[13] M.P. Ormsby, *Turbulent Flame Development in a High-Pressure Combustion Vessel*, Ph.D. Thesis, University of Leeds, 2005.

[14] D. Bradley, R.A. Hicks, M. Lawes, C.G.W. Sheppard, R. Woolley, *Combust. Flame* 115 (1998) 126–144.

[15] F. Creta, M. Matalon, *J. Fluid Mech.* 680 (2011) 225–264.

[16] D. Bradley, C.G.W. Sheppard, R. Woolley, D.A. Greenhalgh, R.D. Lockett, *Combust. Flame* 122 (2000) 195–209.

[17] D. Bradley, Twenty-Fourth Symposium (International) on Combustion, The Combustion Institute, 1992, pp. 247–262.

[18] D. Bradley, *Combust. Theor. Model.* 6 (2002) 361–382.

[19] H. Kobayashi, T. Tamura, K. Maruta, T. Niioka, F. Willams, *Proc. Combust. Inst.* 26 (1996) 389–396.

[20] H. Kobayashi, Y. Kawabata, K. Maruta, *Proc. Combust. Inst.* 27 (1998) 941–948.

[21] D. Bradley, P.H. Gaskell, X.J. Gu, A. Sedaghat, *Combust. Flame* 143 (2005) 227–245.

[22] A.S. Al-Shahrany, D. Bradley, M. Lawes, Kexin Liu, R. Woolley, *Combust. Sci Technol.* 178 (2006) 1771–1802.

[23] D. Bradley, M. Lawes, Kexin Liu, R. Woolley, *Proc. Combust. Inst.* 31 (2007) 1393–1400.